Size and Charge Characterization of Lipid Nanoparticles for mRNA Vaccines

Camille Malburet, Laurent Leclercq, Jean-François Cotte, Jérôme Thiebaud, Emilie Bazin, Marie Garinot, Hervé Cottet

Size and charge characterization of lipid nanoparticles for mRNA vaccines

Camille Malburet[1,2], Laurent Leclercq[1], Jean-François Cotte[2], Jérôme Thiebaud[2], Emilie Bazin[2], Marie Garinot[2], Hervé Cottet[1*]

[1] IBMM, University of Montpellier, CNRS, ENSCM, Montpellier, France

[2] Sanofi Pasteur, 1541 avenue Marcel Mérieux, 69280 Marcy l'Etoile, France

[*] Corresponding author: herve.cottet@umontpellier.fr

ABSTRACT:

Messenger RNA vaccines have come into the spotlight as a promising and adaptive alternative to conventional vaccine approaches. The efficacy of mRNA vaccines relies on the ability of mRNA to reach the cytoplasm of cells, where it can be translated into proteins of interest allowing to trigger the immune response. However, unprotected mRNA is unstable, susceptible to degradation by exo and endonucleases, and its negative charges are electrostatically repulsed by the anionic cell membranes. Therefore, mRNA needs a delivery system that protects the nucleic acid from degradation and allows it to enter into the cells. Lipid nanoparticles (LNPs) represent the non-viral leading vector for mRNA delivery. Physicochemical parameters of LNPs, including their size and their charge, directly impact their *in vivo* behavior and, therefore, their cellular internalization. In this work, Taylor Dispersion Analysis (TDA) was used as a new methodology for the characterization of the size and polydispersity of LNPs, and capillary electrophoresis (CE) was used for the determination of LNPs global charge. The results obtained were compared with those obtained by dynamic light scattering (DLS) and Laser Doppler Electrophoresis (LDE).

INTRODUCTION

mRNA (messenger ribonucleic acid) was discovered in 1961, eight years after DNA (deoxyribonucleic acid).[1] In the first decades after its discovery, the main focus was on understanding its structural and functional aspects. In 1990, Wolff et al. demonstrated that direct injection of *in vitro* transcribed (IVT) mRNA into mice skeletal muscle resulted in the expression of the protein encoded by the mRNA.[2] For the first time, the possibility of using IVT mRNA for therapeutic purposes was shown. Unlike strategies based on plasmid DNA, mRNA does not need to enter into the cell nucleus but only into the cytoplasm to be translated into proteins of interest by ribosomes, allowing to trigger the immune response.[3] Since then, mRNA has shown promise for the treatment of a wide range of diseases and different types of cancer.[4–7] These advances have been enabled by a better understanding of the structure of IVT mRNA, as well as the development of new delivery system.[8] Lipid nanoparticles (LNPs) are currently the most clinically advanced non-viral delivery vehicle for RNA-based drugs.[9] The efficacy of mRNA-based vaccines highly depends on the ability of LNPs to enter cells and deliver mRNA. The physicochemical parameters of LNPs including their size, shape, charge and surface composition, directly impact their cellular internalization.[10]

The size of nanovectors is known to affect intracellular delivery and therefore vaccine efficacy.[11,12] Indeed, size has a significant contribution to many functional parameters, in particular it determines the entry route of particles into the cells.[13–16] Furthermore, LNPs size can be optimized to target certain organs.[17–20] Size requirements are therefore highly dependent on the route of administration and the targeted organ. In all cases, LNPs size must be finely characterized. Regulatory agencies such as the World Health Organization[21], the European Commission[22] and the U. S. Food and Drug Administration[23] qualify LNPs size and size distribution as Critical Quality Attributes (CQA) of messenger RNA vaccines products.

Moreover, the regulatory agencies recommend the use of orthogonal methods for LNPs size determination to address technique-related differences.[21,24]

DLS is a rapid method based on the study of Brownian motion of particles in a liquid. However, critical points can limit the precision of the results obtained by DLS: (*i*) the samples must often be strongly diluted, which can destabilize some formulations; (*ii*) the size derived from the scattered light intensity gives more weight to large particles because the scattered intensity scales as the hydrodynamic radius to the power 6[25] and (*iii*) the size distributions are calculated assuming some pattern of particle shape, which is not always accurate. Therefore, DLS is generally only recommended for the control of samples with relatively low polydispersities. Nanoparticle Tracking Analysis (NTA) is another method also based on the analysis of Brownian motion of particles.[26] Many particles are analyzed individually and simultaneously, their hydrodynamic diameters are calculated using the Stokes-Einstein equation. NTA appears to be more accurate than DLS for polydisperse particles and for detecting the presence of aggregates.[27] However, NTA that is based on the same principle as DLS, also shares some similar limitations, such as important dilutions required and restricted resolution for small particles. Otherwise, Cryogenic Transmission Electron Microscopy (Cryo-TEM) has become a leading technology for imaging nanoscale biological samples such as LNPs.[28] Cryo-TEM can reveal detailed size, morphology and structure information at high resolution. Although Cryo-TEM analysis has obvious advantages, the large adoption of Cryo-TEM for the characterization of nanoparticles is hampered by several factors, such as the high cost of imaging systems, the complex sample preparation and the low image acquisition and analysis rate.[25] Moreover, Cryo-TEM images suffer from high background noise, sometimes non-uniform lighting and artefacts, which makes automatic particle identification difficult.

Charge is another crucial physicochemical parameter cited by the regulatory agencies[21–23]. Charge plays a key role in cellular internalization, dictating the transport of objects across biological barriers.[29,30] The charge of the nanocarriers is controlled by the lipids present in the LNPs, in particular ionizable lipids, and by the composition of the aqueous buffer. Ionizable lipids must be positively charged at low pH allowing mRNA complexation during formulation, LNPs self-assembly and endosomal release (likely). In the meantime, these ionizable lipids must be neutral at physiological pH to avoid potential toxic effects due to unwanted interactions.[31–33] Moreover, studies have shown that the charge of nanoparticles can be optimized to target different organs.[34,35] The charge of nanoparticles is mostly determined by Laser Doppler Electrophoresis (LDE) and generally expressed in terms of Zeta potential, which represents the potential difference between the dispersion medium and the stationary layer of fluid attached to the particle.[36] The Zeta potential strongly depends on the pH, temperature and ionic strength of the medium[37,38], and it was reported that the surface charge density can be instead preferably reported[39,40]. Capillary electrophoresis (CE) is another method for determining the surface charge density of nanoparticles.[41] Several studies have focused on the study of the electrophoretic mobility of liposomes.[42–45] It is worth noting that LDE and CE are both based on the determination of electrophoretic mobilities, which are then transformed into Zeta potential and/or surface charge density using electrophoretic mobility modelling. The determination of electrophoretic mobilities by CE requires small sample volumes and the analyses have the advantage of being easily automated. In addition, CE is a separative method allowing getting information on charge density distributions.

In this work, Taylor Dispersion Analysis (TDA) was used as a new alternative method to determine the size and size distribution of LNPs encapsulating mRNA. TDA is an absolute method which requires very little sample, is easily automated and has the advantage to be

performed without any alteration of the sample (analysis performed in the sample matrix). Chamieh et al. used TDA to determine the size of micelles and microemulsions,[46–48] while Franzen et al. used TDA to determine the size of PEGylated liposomal formulations.[42] Moreover, the size distribution of nano-objects can be derived from the experimental Taylorgram using Regularized Linear Inversion (CRLI) approach.[49] To our knowledge, TDA has never been used for the characterization of lipid nanoparticles encapsulating mRNA. This work presents an optimized TDA methodology to access to the size and size distribution of LNPs and a comparison with the results obtained by DLS. Using the same equipment, the charge of the lipid nanoparticles was determined by capillary electrophoresis and the results were compared with those obtained by LDE.

EXPERIMENTAL SECTION

Chemicals and Materials. FLuc (Cyanine 5 Firefly Luciferase) mRNA (1929 nucleotides) was purchased from TriLink BioTechnologies (San Diego, USA). DLin-MC3-DMA ((6Z,9Z,28Z,31Z)-heptatriacont-6,9,28,31-tetraene-19-yl 4-(dimethylamino)butanoate) was purchased from Sai Life Sciences Ltd. (Telangana, India). DSPC (1,2-distearoyl-sn-glycero-3-phosphocholine), Chol (cholesterol), DMG-PEG-2000 (1,2-dimyristoyl-rac-glycero-3-methoxypolyethylene glycol-2000), trisodium citrate dihydrate $HOC(COONa)(CH_2COONa)_2 \cdot 2H_2O$, ($M_w$ = 294.1 g/mol), citric acid monohydrate $HOC(COOH)(CH_2COOH)_2 \cdot$ H2O (M_w = 210.1 g/mol) and Hellmanex III were purchased from Sigma-Aldrich (St. Quentin Fallavier, France). PBS (phosphate-buffered saline) 10X buffer was purchased from Eurobio Scientific (Les Ulis, France). Absolute ethanol was purchased from Carlo Erba Reagents (Val de Reuil, France). Bare fused silica capillaries were purchased from Molex Polymicro Technologies (Phoenix, USA). µSIL-FC (fluorocarbon polymer), PVA (polyvinyl alcohol), DB-1

(polydimethylsiloxane) and DB-WAX (polyethylene glycol) coated capillaries were purchased from Agilent Technologies (Santa Clara, USA). Ultratrol LN was purchased from Target Discovery (Santa Clara, USA). PEO (poly(ethylene oxide), M_v ~ 4,000,000 Da), DLPC (1,2-dilauroyl-sn-glycero-3-phosphocholine) and DDAB (dimethyldioctadecylammonium bromide salt) were purchased from Sigma-Aldrich (St. Quentin Fallavier, France). DMF (dimethylformamide) was purchased from Carlo Erba Reagents (Val-de-Reuil, France). Deionized water was further purified with a Milli-Q system from Millipore (Molsheim, France).

Formulation of LNPs. The formulation of LNPs involved the rapid mixing of an ethanolic phase composed of DLinMC3-DMA:DSPC:Chol:DMG-PEG-2000 (50:10:38.5:1.5 molar ratio, see Figure S1 for the molecular structure of the LNP constituents) with a 50 mM citrate aqueous phase at pH 4 containing the mRNA at 0.25 mg/mL. Stock solutions of lipids were previously prepared in absolute ethanol at the following concentrations: DLinMC3-DMA 100 mg/mL, DSPC 30 mg/mL, Chol 18 mg/mL, DMG-PEG-2000 30 mg/mL. The mixture was carried out using a NanoAssemblr® system from Precision NanoSystems (Vancouver, Canada) at 4 mL/min total flow rate with 3:1 (aqueous phase:ethanolic phase) flow rate ratio. After formulation, 3 dialysis steps were carried out in order to remove ethanol from the formulation and raise the pH to physiological in PBS buffer, 3.2 mL of mRNA-LNP solution were recovered after the last dialysis step.

Taylor Dispersion Analysis (TDA). All experiments were carried out on a 7100 CE Agilent system (Waldbronn, Germany). This system is equipped with a diode array detector (DAD). All the measurements were performed at 200 nm. The temperature of the capillary cartridge was set at 25°C. The LNPs formulations were injected without prior dilution into the capillaries filled with PBS buffer. TDA experiments were performed using 60 mbar mobilization

pressure of a sample plug injected at 20 mbar for 6 s. The elution peak obtained was fitted using the sum of two Gaussians according to equation (1) using a home-developed Excel spreadsheet and Excel solver:

$$S(t) = \frac{A_1}{\sigma_1\sqrt{2\pi}} exp \frac{-(t-t_0)^2}{2{\sigma_1}^2} + \frac{A_2}{\sigma_2\sqrt{2\pi}} exp \frac{-(t-t_0)^2}{2{\sigma_2}^2} \quad (1)$$

where $S(t)$ is the absorbance signal, t_0 is the average elution time, σ_1 and σ_2 are the temporal variances and A_1 and A_2 are two constants that depended on the response factor and the injected quantity of solute. σ_1, σ_2, A_1 and A_2 are four adjusting parameters obtained by nonlinear least square regression. t_0 is directly obtained from the position of the maximum absorbance. One of the two populations (the largest in size) represents the LNPs, and the other (the smallest) represents the presence of detected small molecules.

The temporal variance σ_i derived from the elution profile allows to calculate the molecular diffusion coefficient D_i of each population according to equation (2), from which the hydrodynamic diameter $D_{h,i}$ can be determined using Stokes–Einstein equation (3):

$$D_i = \frac{R_c^2 t_0}{24{\sigma_i}^2} \quad (2)$$

where R_c is the capillary radius.

$$D_{h,i} = \frac{k_B T}{6\pi\eta D_i} \quad (3)$$

where k_B is the Boltzmann constant, T is the temperature, and η is the eluent viscosity.

To go further in the data analysis of the Taylorgram, the elution profile was fitted using a second approach based on Regularized Linear Inversion (CRLI) algorithm[49] to get a continuous distribution of the diffusion coefficient or of the hydrodynamic radius according to equation (4):

$$S(t) = \int_0^\infty CM(D)\rho(D)\sqrt{D}\, exp\left[\frac{-(t-t_0)^2 12D}{{R_c}^2 t_0}\right] dD \quad (4)$$

where *C* is an instrumental constant, *M(D)* and *ρ(D)* are the mass and the molar concentration of the objects with the diffusion coefficient *D*, respectively. The polydispersity of the sample can be determined using equations (5) and (6):

$$\sigma_{D_h}{}^2 = \frac{\int_{D_{hmin}}^{D_{hmax}} (D_h - \overline{D_h})^2 P(D_h) dD_h}{\int_{D_{hmin}}^{D_{hmax}} P(D_h) dD_h} \quad (5)$$

$$PDI = \left(\frac{\sigma_{D_h}}{\overline{D_h}}\right)^2 \quad (6)$$

Dynamic Light Scattering (DLS) and Laser Doppler Electrophoresis (LDE). All experiments were carried out on a Malvern Panalytical Zetasizer Nano ZS system (Palaiseau, France). For both analyses, the temperature of the cuvettes was set at 25°C. For DLS measurements, the LNPs formulations were diluted by adding 10 µL of the formulation into 1 mL PBS buffer prior to analysis. DLS experiments were performed using 173° measurement angle. Cumulant fit was used to fit the experimental data of the autocorrelation function. For LDE measurements, the LNPs formulations were diluted by adding 100 µL of the formulation into 400 µL PBS buffer prior to analysis.

Capillary Electrophoresis. All experiments were carried out on a 7100 CE Agilent system (Waldbronn, Germany) equipped with a diode array detector (DAD). µSIL-FC capillaries of 50 cm total length (41.5 cm to the UV detector) × 50 µm i.d. were used. The temperature of the capillary cartridge was set at 25°C. The capillaries were presaturated before use with LNPs formulations for 10 min at 60 mbar. Before each sample injection the capillaries were flushed for 2 min with Mili-Q water at 960 mbar followed by 2 min 10 mM PBS at 960 mbar. LNPs samples were hydrodynamically injected with 20 mbar pressure for 6 s. CE experiment were performed applying 14 kV voltage and 7 mbar pressure. The UV detection was performed at 200 nm.

RESULTS AND DISCUSSION

Lipid nanoparticles (LNPs) are usually composed of four lipids serving to encapsulate mRNA: an ionizable lipid, a phospholipid, cholesterol, and a PEG-lipid, as schematically depicted in Figure 1. The ionizable lipid used in this study was DLin-MC3-DMA, which is often used as a reference after its success in the first RNA-based drug (named ONPATTRO® (patisiran)) approved by the Food and Drug Administration (FDA) and the European Medicines Agency (EMA) in 2018.[50] This drug uses siRNAs encapsulated into LNPs for the treatment of hereditary transthyretin-mediated (hATTR) amyloidosis.[51,52] Ionizable lipids are positively charged at low pH, allowing mRNA complexation, and are neutral at physiological pH reducing potential toxic effects.[53] The phospholipid used in this study was DSPC, whose role is to increase the stability of the LNPs.[54] The PEG-lipid used was DMG-PEG-2000, whose incorporation in LNPs increases their colloidal stability and their resistance to *in vivo* opsonization and clearance.[54] Finally, cholesterol provided structural integrity to the LNPs.[33,54] The inclusion of cholesterol in nanoparticle formulations has also been shown to improve efficacy, potentially due to improved membrane fusion allowing endosomal release.[33,55,56] The chemical formulas of the different lipids are given in Figure S1.

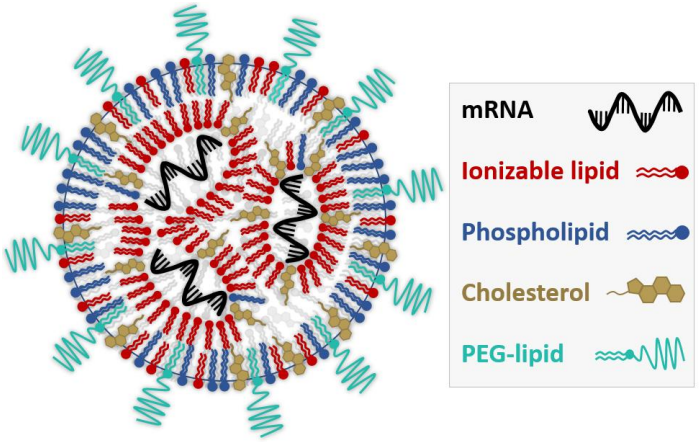

206
207 **Figure 1.** Hypothetical structure of mRNA-LNPs. The PEG-lipid along with DSPC resides
208 primarily on the LNPs surface, while the ionizable lipid and cholesterol are distributed
209 throughout the LNPs. [57,58]
210

After formulation, the first step of this work was to perform a screening of different

coated capillaries in order to select the appropriate coating for the analysis of LNPs. Bare fused

213 silica and DB-1 (polydimethylsiloxane), DB-WAX (PEG), µSIL-FC (fluorinated polymer) and

PVA coated capillaries are commercial capillaries. PEO, Ultratrol LN and DLPC-DDAB coated

215 capillaries were dynamically produced according to the protocols described in Section 2 of the

Supporting Information. A plug of LNPs formulation was first injected into the different

217 capillaries after simply rinsing the capillaries with PBS buffer. Results are presented in Figure

2A. It appears that without presaturation of the capillary with the LNPs formulation, DB-WAX coating was the only capillary coating that allowed to observe a symmetrical Taylorgram. Yet, this coating was not retained, due to relatively poor repeatability of the measurements. A very important absorption was observed on all the other capillaries. It is interesting to note that no peak was observed on silica, DB1 and µSIL capillaries, suggesting that the injected sample was totally adsorbed on the capillary wall. On the contrary, after presaturation of the capillaries by performing a pre-frontal injection of LNPs formulations (60 mbar for 10 min), a peak was observed on all the different capillaries (see Figure 2B). The presaturation allows to saturate the interaction sites within the capillary surface and creates a dynamic coating inside the capillary. For all the studied coated capillaries, the peak appeared more symmetrical after presaturation,

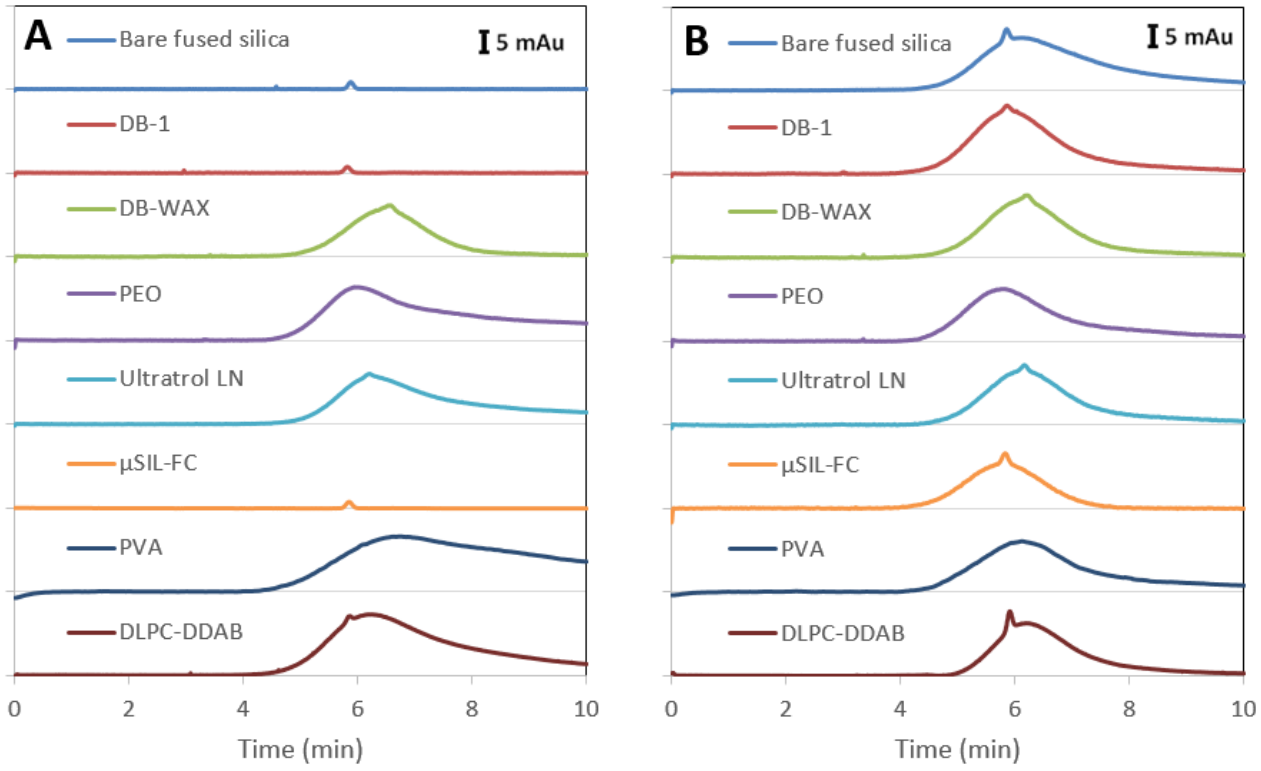

suggesting a reduced LNP adsorption. The coating which was selected for the rest of the study was the µSIL-FC coating, as it gave the most symmetrical gaussian peak and the best baseline return after presaturation (see Figure 2B).

Figure 2. Screening of different capillary coatings without capillary presaturation (A) and with capillary presaturation (B). Experimental conditions: 50 cm total length (41.5 cm to the UV detector) × 50 µm i.d. capillaries. Buffer: PBS, pH 7.4. Capillary conditioning: H_2O for 2 min at 960 mbar followed by 2 min PBS at 960 mbar (A), H_2O for 2 min, LNP for 10 min at 60 mbar followed by 2 min PBS at 960 mbar (B). Injection of LNP: 20 mbar, 6 s. Mobilization pressure: 60 mbar. Sample: lipid nanoparticles (DLin-MC3-DMA:DSPC:Chol:DMG-PEG-2000 at 50:10:38.5:1.5 molar ratio) encapsulating Firefly Luciferase (FLuc) mRNA. UV detection: 200 nm. Temperature: 25°C.

Capillary conditioning: H_2O for 2 min at 960 mbar followed by 2 min PBS at 960 mbar.

In order to improve the repeatability of the measurements, rinsing steps were also optimized. Between two successive runs, capillaries were simply rinsed for 1 min with water and 2 min with PBS buffer. The repeatability of 10 successive runs was shown in Figure 3A. After each analysis sequence capillaries were rinsed for 5 min with 1% Hellmanex in water, 10 min with isopropanol and 5 min with water. Capillaries were presaturated again at the start of each new sequence by injecting a front of the sample (60 mbar for 10 min).

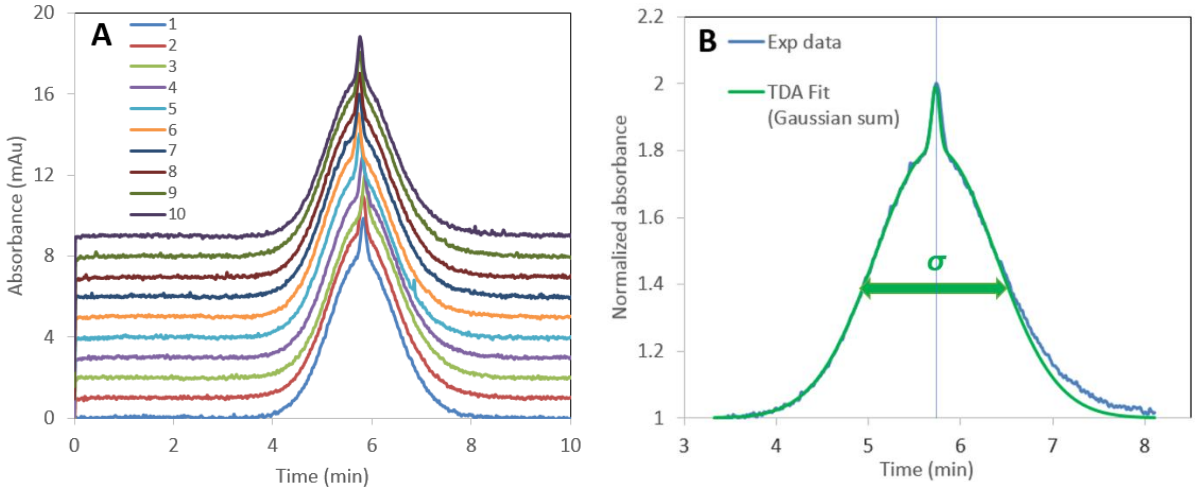

Figure 3. Repeatability on 10 successive runs (A) and an example of two-Gaussian fit (B) of the Taylorgrams obtained for LNP size characterization. Experimental conditions: µSIL-FC coated capillaries of 50 cm total length (41.5 cm to the UV detector) × 50 µm i.d. Buffer: 10 mM PBS, pH 7.4, η = 0.9×10^{-3} Pa.s. Capillary presaturation: LNP for 10 min at 60 mbar. Capillary preconditioning: H_2O for 2 min at 960 mbar followed by 2 min PBS at 960 mbar. Injection of LNP: 20 mbar, 6 s. Mobilization pressure: 60 mbar. Sample: lipid nanoparticles (DLin-MC3-DMA:DSPC:Chol:DMG-PEG-2000 at 50:10:38.5:1.5 molar ratio) encapsulating Firefly Luciferase (FLuc) mRNA. UV detection: 200 nm. Temperature: 25°C.

Figure 3B displays an example of two-Gaussian fit obtained for one repetition of the LNP sample. The two-Gaussian fit was performed only on the left half of the elution peak to avoid any impact of peak tailing on the size measurement. Two-Gaussian fit was required due to the presence of UV absorbing small molecules in the LNP sample, appearing as the small peak on the top of the signal. The calculation of the LNP hydrodynamic diameter requires to know the viscosity of the analysis buffer, which can be easily derived by measuring the elution time of UV absorbing marker in a prefilled capillary (see section 3 in Supporting Information for more details). Using the determined viscosity of PBS (η = 0.90 10^{-3} $Pa.s^{-1}$), the hydrodynamic diameter obtained by Gaussian fit for the LNPs analyzed by TDA was 86 ± 1 nm (average over the 10 runs presented in Figure 3).

A more advanced data processing of the Taylorgram based on Regularized Linear Inversion (CRLI) algorithm[49] was performed to get a continuous distribution of the diffusion coefficient (see Figure S3 for example of experimental fit). The size distribution could be determined by CRLI as exemplified in Figure 4A.

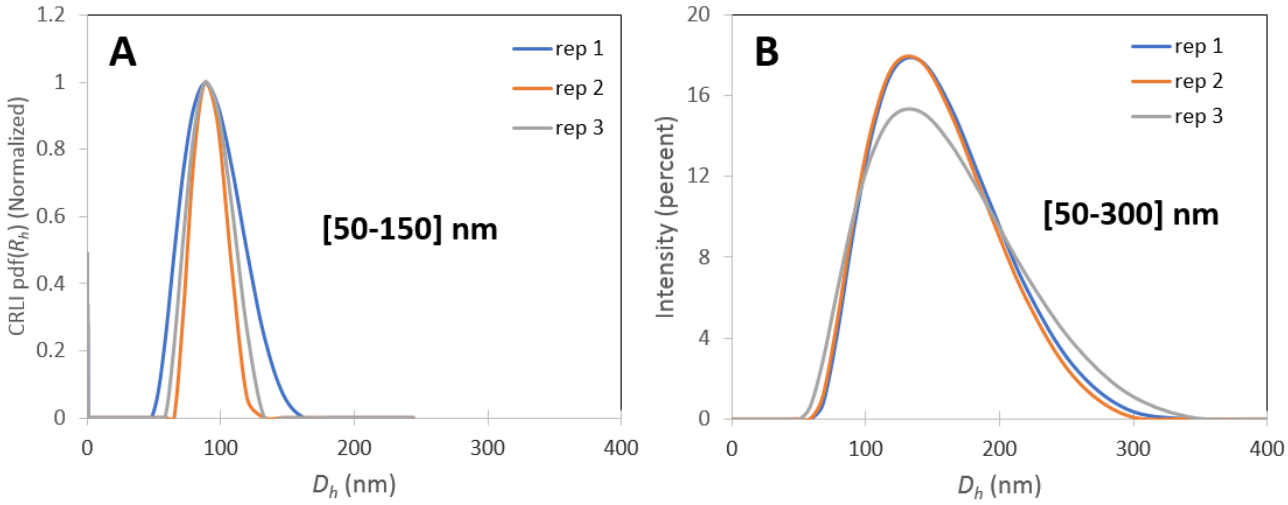

Figure 4. Size distributions (three repetitions) obtained by TDA (A) and by DLS (B). Same experimental conditions for TDA as in Figure 3. Experimental conditions for DLS: 10 µL LNP solution into 1 mL of 10 mM PBS, pH 7.4, η = 0.9×10^{-3} Pa.s. Measurement angle: 173°C. Temperature: 25°C.

The size distributions obtained by TDA (CRLI) were compared with those obtained by DLS using Cumulant fit (Figure 4B). The size distributions obtained by DLS [50-300 nm] were wider than those obtained in TDA [50-150 nm]. Accordingly, the mean hydrodynamic diameter obtained by DLS was higher than the one obtained by TDA (128 ±1 nm *vs* 86 ±1) and the polydispersity index was higher in DLS than in TDA (0.112 *vs* 0.011). These differences can be explained by the fact that the two techniques are not sensitive to the same size distributions. Intensity average distributions obtained by DLS give more weight to the larger entities (see Figure 5), since the distribution is weighted by the scattered intensity which basically scales as the hydrodynamic radius to the power 6. In contrast, the size distribution derived from TDA is basically related to the weight-average distribution, which means that each LNP should contribute to the distribution in proportion to their mass content in the mixture. To stress the

differences between the two methods, an example of the differently weighted distributions is provided in Figure 5 taking as an example a bimodal mixture containing 5% in number of large particles (200 nm) and 95% of smaller one (80 nm), which could mimic an example of LNP mixture containing a minor content of larger particles. Clearly, the intensity-based distribution (DLS) is weighting more the larger particles than the weight counterpart (TDA). These differences demonstrate the complementarity of the two techniques which do not determine the same size distributions. Of course, for truly monodisperse samples, both techniques should converge; otherwise the discrepancy between the average values and the distributions are indicative of the sample size heterogeneity. However, it should be noted that it is generally not straightforward to convert the intensity based DLS distribution into a mass-weighted (or a number-weighted) size distribution because the scattered intensity is depending on the size and the shape of the solutes[59]. For such transformations, strong assumptions are required such as the spherical shape and the homogeneity of the solutes, and may be restricted to a limited range of sizes. Moreover, due to the intensity based response of the light scattered intensity, the signal due to the smallest solutes can be so weak that it is not detected, especially in the case of polydisperse samples. This is a reason why orthogonal sizing methods are requested by the regulation authorities in the case of polydisperse samples.

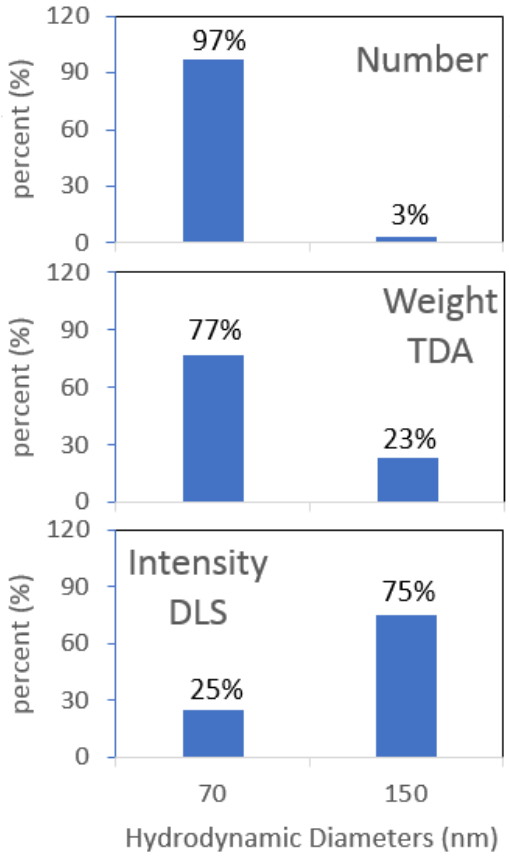

Figure 5. Distributions in number, in weight (as determined by TDA for mass sensitive detection) and in intensity (as determined by DLS) considering a bimodal mixture containing 3% in number of large particles (150 nm) and 97% of smaller ones (70 nm). The mass proportion, obtained in TDA for mass sensitive detection, is proportional to the number of particles multiplied by the hydrodynamic size to the power 3 (volume). We assume as a first approximation that the density of the particles is the same for both particle sizes. The scattered intensity obtained in DLS is proportional to the number of particles multiplied by the hydrodynamic size to the power 6.

Finally, the charge of the LNPs was studied by capillary electrophoresis (CE) using a µSIL coated capillary as for TDA analysis. Figure 6A displays a Taylorgram (no electric field, see blue trace) where the marker (DMF at 0.1 g/L in water) is detected at the same elution time as the LNPs, but with a narrower profile compared to the broad LNP elution profile. By applying an electric field and reducing the mobilization pressure from 30 mbar (orange trace) to 7 mbar (green trace), it was possible to separate the two peaks and to calculate the effective electrophoretic mobility of the LNPs (μ_{ep}= -1.86×10^{-9} m^{2}V^{-1}s^{-1}). The applied co-pressure (7

mbar) allows to speed up the analysis with a limited impact on the peak broadening of the LNPs peak, and without changing the LNP effective mobility. Knowing the hydrodynamic diameter and the electrophoretic mobility of LNPs, it was possible to calculate the electric charge density (σ_{OWO}) using the O'Brien-White-Ohshima (OWO) mathematical model[39,60,61], according to equation (7):

$$\sigma_{OWO} = \frac{2\varepsilon_0\varepsilon_r\kappa k_B T}{e}\sinh\left(\frac{e\zeta}{2k_B T}\right)\times\left[1+\frac{1}{\kappa R_h}\frac{2}{\cosh^2(\frac{e\zeta}{4k_B T})}+\frac{1}{(\kappa R_h)^2}\frac{8\ln(\cosh(\frac{e\zeta}{4k_B T}))}{\sinh^2(\frac{e\zeta}{2k_B T})}\right]^{\frac{1}{2}} \quad (7)$$

where ε_r is the relative electric permittivity, ε_0 is the electric permittivity of vacuum, e is the elementary electric charge, ζ is the Zeta potential and κ is the Debye–Hückel parameter (κ = 1.28 nm^{-1}, 165 mM ionic strength in the present work). The surface charge density is the total surface charge of the particle divided by the total surface of the particle at the plane of shear. The determination of σ_{OWO} requires the determination of the Zeta potential ζ knowing μ_{ep} and D_h. This can be done using graphical representations of equation (8):

$$\mu_{ep} = \frac{2\varepsilon_0\varepsilon_r\zeta}{3\eta}\left[f_1(\kappa R_h)-\left(\frac{e\zeta}{k_B T}\right)^2 f_3(\kappa R_h)-\frac{m_- + m_+}{2}\left(\frac{e\zeta}{k_B T}\right)^2 f_4(\kappa R_h)\right] \quad (8)$$

m_+ and m_- are dimensionless ionic drag coefficients, accessible from the limiting conductances of the cation Λ_+^0 and the anion Λ_-^0 in the electrolyte considered:

$$m_\pm = \frac{2\varepsilon_0\varepsilon_r k_B T N_A}{3\eta z\Lambda_\pm^0} \quad (9)$$

where N_A is the Avogadro's number and m_+ = 0.263, m_- = 0.172 for NaCl electrolyte. Equation (8) takes the relaxation effect into account and is valid for $\zeta \leq 100$ mV. $f1$, $f3$ and $f4$ are functions given by equations (10), (11) and (12):

$$f_1(\kappa R_h) = 1 + \frac{1}{2\left[1 + 2.5 / \left\{\kappa R_h \left(1 + 2e^{-\kappa R_h}\right)\right\}\right]^3} \quad (10)$$

$$f_3(\kappa R_h) = \frac{\kappa R_h \left(\kappa R_h + 1.3e^{-0.18\kappa R_h} + 2.5\right)}{2\left(\kappa R_h + 1.2e^{-7.4\kappa R_h} + 4.8\right)^3} \quad (11)$$

$$f_4(\kappa R_h) = \frac{9\kappa R_h \left(\kappa R_h + 5.2e^{-3.9\kappa R_h} + 5.6\right)}{8\left(\kappa R_h + 1.55e^{-0.32\kappa R_h} + 6.02\right)^3} \quad (12)$$

Thus, for the formulation of LNPs studied in this work, the Zeta potential determined by graphical representation was ζ_{LNP} = -2.5 mV (see Figure S4 with κR_h = 55), which allowed to calculate the lipid nanoparticles electric charge density, σ_{LNP} = -2.4×10^{-3} Cm^{-2}= - 0.015 elementary charge per nm^2. This negative charge at physiological pH is relatively low but is desired to reduce unwanted interactions during circulation in the body. Such surface charge density corresponds to an overall effective charge of about 350 elementary charges per LNP entity. Because the charge density is low, relaxation phenomena is expected to be negligible, and it is therefore possible to apply the approximated Henry equation, which is a more straightforward way to determine the Zeta potential from the effective electrophoretic mobility using eq. (13)[62]:

$$\mu_{ep} = \frac{2\varepsilon\zeta}{3\eta} \times \left(1 + \frac{1}{2\left(1 + \frac{\delta}{\kappa R_h}\right)^3}\right) \quad (13)$$

where $\delta = \frac{2.5}{1+2\exp(-\kappa R_h)}$. Numerical application to LNP leads to δ=2.5, $\mu_{ep} = \frac{0.958\varepsilon\zeta}{\eta}$, ζ_{LNP} = -2.47 mV and finally to the same values of σ_{LNP} = -2.4×10^{-3} Cm^{-2}= - 0.015 elementary charge per nm^2 as those previously obtained with OWO modeling.

It is worth noting that the surface charge density is a much more robust parameter to characterize solute charge compared to Zeta potential, as previously demonstrated for nanoparticles and nanolatexes.[39,40] Indeed, Zeta potential is strongly dependent on the ionic strength due to the compaction of the electrical double layer with increasing ionic strength, which is not the case for surface charge density[39,40]. The electrophoretic mobility value obtained by CE can also be compared to the one determined by Laser Doppler electrophoresis (LDE) μ_{ep}= -5.00×10^{-9} m²V^{-1}s^{-1}, which is of the same order of magnitude as the one determined by CE (μ_{ep}= -1.86×10^{-9} m²V^{-1}s^{-1}) and allows to determine the Zeta by graphical representation using OWO model ζ_{LNP} = -6.5 mV, see Figure S4. The difference between the two values can nevertheless be explained by the fact that the electrophoretic mobility determined by LDE strongly depends on the other ions present in the matrix since LDE is a non-separative method.

It is worth noting that it is also important to know which electrophoretic modelling is used to convert the effective mobility into Zeta potential and at which ionic strength the measurement was performed. Strong differences can arise depending on the retained modelling (Nernst-Einstein, Hückel, Smolukowski, Henry, OWO, modified Yoon and Kim modelling) depending on the solute's characteristics. OWO and modified Yoon and Kim modelling are the most accurate one since they take into account both the electrophoretic effect (counter ion friction) and the relaxation effect (distortion of the counterion cloud)[61]. We also recommend, for the reasons

previously explained, to express all the results in terms of surface charge density using equation (7) instead of Zeta potential.

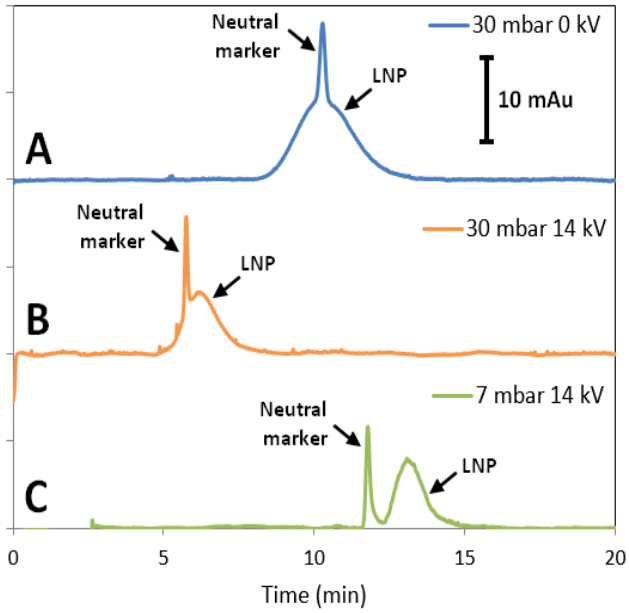

Figure 6. Taylorgram (A) and electropherograms (B, C) obtained for a mixture of LNP and DMF. Experimental conditions: µSIL-FC capillaries of 50 cm total length (41.5 cm to the UV detector) × 50 µm i.d. Buffer: 10 mM PBS, pH 7.4, η = 0.9×10^{-3} Pa.s.. Capillary presaturation: LNP for 10 min at 60 mbar. Capillary preconditioning: H_2O for 2 min at 960 mbar followed by 2 min PBS at 960 mbar. Injection of LNP: 20 mbar, 6 s. Mobilization pressure and separation voltage: as indicated on the graph. Sample: lipid nanoparticles (DLin-MC3-DMA:DSPC:Chol:DMG-PEG-2000 at 50:10:38.5:1.5 molar ratio) encapsulating Firefly Luciferase (FLuc) mRNA. UV detection: 200 nm. Temperature: 25°C.

CONCLUSIONS

This work aimed at developing a new methodology to characterize the average size and the size distribution, as well as the charge density, of lipid nanoparticles (LNPs) used as delivery vehicle for mRNA vaccines. The TDA method developed in this work was found to reach this goal with direct injection of the samples (no dilution, no filtration). It appeared that the presaturation of the capillary with the LNP sample and the capillary rinsing were crucial steps that significantly decreased the adsorption of LNPs onto the capillary wall and considerably improved the

repeatability. The comparison between TDA and DLS shows that the hydrodynamic diameters obtained by TDA were smaller (mass-weighted) than those obtained by DLS (intensity-weighted), as expected. Both methods are therefore complementary and allow a better characterization of the LNP size. TDA shows promise to be widely used as it is an absolute method (no calibration) that consumes little sample volumes, it is easy and straightforward to use, and it can be easily automated. TDA performed on a CE equipment can also easily provide the viscosity of LNPs formulations, which can be useful when low amounts of product are available. Finally, CE, implemented on the same equipment as TDA, can be used for the charge characterization of LNPs using O'Brien-White-Ohshima or Henry electrophoretic mobility modelling. Thus, a single equipment can give access to important information on critical LNPs physicochemical parameters.

ASSOCIATED CONTENT

Supporting Information. Chemical formula of the 4 lipids used in the formulation of the lipid nanoparticles. PEO, Ultratrol LN and DDAB-DLPC capillary coatings procedures. Calculation of the viscosity of PBS and LNP solutions. CRLI Fit.

DISCLOSURES

This work was partly funded by Sanofi Pasteur under a Cooperative Research and Development Agreement with the University of Montpellier and the CNRS.

REFERENCES

(1) Brenner, S.; Jacob, F.; Meselson, M. An Unstable Intermediate Carrying Information from Genes to Ribosomes for Protein Synthesis. *Nature* **1961**, *190* (4776), 576–581. https://doi.org/10.1038/190576a0.

(2) Wolff, J.; Malone, R.; Williams, P.; Chong, W.; Acsadi, G.; Jani, A.; Felgner, P. Direct Gene Transfer into Mouse Muscle in Vivo. *Science* **1990**, *247* (4949), 1465–1468. https://doi.org/DOI:10.1126/science.1690918.

(3) Liu, M. A. A Comparison of Plasmid DNA and MRNA as Vaccine Technologies. *Vaccines* **2019**, *7* (2), 37. https://doi.org/10.3390/vaccines7020037.
(4) Jirikowski, G.; Sanna, P.; Maciejewski-Lenoir, D.; Bloom, F. Reversal of Diabetes Insipidus in Brattleboro Rats: Intrahypothalamic Injection of Vasopressin MRNA. *Science* **1992**, *255* (5047), 996. https://doi.org/10.1126/science.1546298.
(5) Schirrmacher, V.; Förg, P.; Dalemans, W.; Chlichlia, K.; Zeng, Y.; Fournier, P.; von Hoegen, P. Intra-Pinna Anti-Tumor Vaccination with Self-Replicating Infectious RNA or with DNA Encoding a Model Tumor Antigen and a Cytokine. *Gene Ther.* **2000**, *7* (13), 1137–1147. https://doi.org/10.1038/sj.gt.3301220.
(6) Ramaswamy, S.; Tonnu, N.; Tachikawa, K.; Limphong, P.; Vega, J. B.; Karmali, P. P.; Chivukula, P.; Verma, I. M. Systemic Delivery of Factor IX Messenger RNA for Protein Replacement Therapy. *Proc. Natl. Acad. Sci.* **2017**, *114* (10), E1941. https://doi.org/10.1073/pnas.1619653114.
(7) Pardi, N.; Secreto, A. J.; Shan, X.; Debonera, F.; Glover, J.; Yi, Y.; Muramatsu, H.; Ni, H.; Mui, B. L.; Tam, Y. K.; Shaheen, F.; Collman, R. G.; Karikó, K.; Danet-Desnoyers, G. A.; Madden, T. D.; Hope, M. J.; Weissman, D. Administration of Nucleoside-Modified MRNA Encoding Broadly Neutralizing Antibody Protects Humanized Mice from HIV-1 Challenge. *Nat. Commun.* **2017**, *8* (1), 14630. https://doi.org/10.1038/ncomms14630.
(8) Hajj, K. A.; Whitehead, K. A. Tools for Translation: Non-Viral Materials for Therapeutic MRNA Delivery. *Nat. Rev. Mater.* **2017**, *2* (10), 17056. https://doi.org/10.1038/natrevmats.2017.56.
(9) Davies, N.; Hovdal, D.; Edmunds, N.; Nordberg, P.; Dahlén, A.; Dabkowska, A.; Arteta, M. Y.; Radulescu, A.; Kjellman, T.; Höijer, A.; Seeliger, F.; Holmedal, E.; Andihn, E.; Bergenhem, N.; Sandinge, A.-S.; Johansson, C.; Hultin, L.; Johansson, M.; Lindqvist, J.; Björsson, L.; Jing, Y.; Bartesaghi, S.; Lindfors, L.; Andersson, S. Functionalized Lipid Nanoparticles for Subcutaneous Administration of MRNA to Achieve Systemic Exposures of a Therapeutic Protein. *Mol. Ther. - Nucleic Acids* **2021**, *24*, 369–384. https://doi.org/10.1016/j.omtn.2021.03.008.
(10) Kim, J.; Eygeris, Y.; Gupta, M.; Sahay, G. Self-Assembled MRNA Vaccines. *Adv. Drug Deliv. Rev.* **2021**, *170*, 83–112. https://doi.org/10.1016/j.addr.2020.12.014.
(11) Jiang, W.; Kim, B. Y. S.; Rutka, J. T.; Chan, W. C. W. Nanoparticle-Mediated Cellular Response Is Size-Dependent. *Nat. Nanotechnol.* **2008**, *3* (3), 145–150. https://doi.org/10.1038/nnano.2008.30.
(12) Hoshyar, N.; Gray, S.; Han, H.; Bao, G. The Effect of Nanoparticle Size on in Vivo Pharmacokinetics and Cellular Interaction. *Nanomed.* **2016**, *11* (6), 673–692. https://doi.org/10.2217/nnm.16.5.
(13) Conner, S. D.; Schmid, S. L. Regulated Portals of Entry into the Cell. *Nature* **2003**, *422* (6927), 37–44. https://doi.org/10.1038/nature01451.
(14) Rejman, J.; Oberle, V.; Zuhorn, I. S.; Hoekstra, D. Size-Dependent Internalization of Particles via the Pathways of Clathrin- and Caveolae-Mediated Endocytosis. *Biochem. J.* **2004**, *377* (Pt 1), 159–169. https://doi.org/10.1042/BJ20031253.
(15) Petros, R. A.; DeSimone, J. M. Strategies in the Design of Nanoparticles for Therapeutic Applications. *Nat. Rev. Drug Discov.* **2010**, *9* (8), 615–627. https://doi.org/10.1038/nrd2591.
(16) Andar, A. U.; Hood, R. R.; Vreeland, W. N.; DeVoe, D. L.; Swaan, P. W. Microfluidic Preparation of Liposomes to Determine Particle Size Influence on Cellular Uptake Mechanisms. *Pharm. Res.* **2014**, *31* (2), 401–413. https://doi.org/10.1007/s11095-013-1171-8.
(17) Chauhan, V. P.; Jain, R. K. Strategies for Advancing Cancer Nanomedicine. *Nat. Mater.* **2013**, *12* (11), 958–962. https://doi.org/10.1038/nmat3792.
(18) Le-Vinh, B.; Steinbring, C.; Wibel, R.; Friedl, J. D.; Bernkop-Schnürch, A. Size Shifting of Solid Lipid Nanoparticle System Triggered by Alkaline Phosphatase for Site Specific Mucosal Drug Delivery. *Eur. J. Pharm. Biopharm.* **2021**, *163*, 109–119. https://doi.org/10.1016/j.ejpb.2021.03.012.

(19) Mitchell, M. J.; Billingsley, M. M.; Haley, R. M.; Wechsler, M. E.; Peppas, N. A.; Langer, R. Engineering Precision Nanoparticles for Drug Delivery. *Nat. Rev. Drug Discov.* **2021**, *20* (2), 101–124. https://doi.org/10.1038/s41573-020-0090-8.

(20) Blanco, E.; Shen, H.; Ferrari, M. Principles of Nanoparticle Design for Overcoming Biological Barriers to Drug Delivery. *Nat. Biotechnol.* **2015**, *33* (9), 941–951. https://doi.org/10.1038/nbt.3330.

(21) World Health Organization. Evaluation of the Quality, Safety and Efficacy of Messenger RNA Vaccines for the Prevention of Infectious Diseases: Regulatory Considerations. 2021.

(22) EU Official Control Authority. Official Control Authority Batch Release Of Pandemic COVID-19 Vaccine (MRNA). 2021.

(23) U.S. FDA. Liposome Drug Products: Chemistry, Manufacturing, and Controls; Human Pharmacokinetics and Bioavailability; and Labeling Documentation. 2018.

(24) U.S. FDA. Drug Products, Including Biological Products, That Contain Nanomaterials-Guidance for Industry. 2017.

(25) Crawford, R.; Dogdas, B.; Keough, E.; Haas, R. M.; Wepukhulu, W.; Krotzer, S.; Burke, P. A.; Sepp-Lorenzino, L.; Bagchi, A.; Howell, B. J. Analysis of Lipid Nanoparticles by Cryo-EM for Characterizing SiRNA Delivery Vehicles. *Int. J. Pharm.* **2011**, *403* (1), 237–244. https://doi.org/10.1016/j.ijpharm.2010.10.025.

(26) Rozo, A. J.; Cox, M. H.; Devitt, A.; Rothnie, A. J.; Goddard, A. D. Biophysical Analysis of Lipidic Nanoparticles. *Membr. Protein Tools Drug Discov.* **2020**, *180*, 45–55. https://doi.org/10.1016/j.ymeth.2020.05.001.

(27) Filipe, V.; Hawe, A.; Jiskoot, W. Critical Evaluation of Nanoparticle Tracking Analysis (NTA) by NanoSight for the Measurement of Nanoparticles and Protein Aggregates. *Pharm. Res.* **2010**, *27* (5), 796–810. https://doi.org/10.1007/s11095-010-0073-2.

(28) Kulkarni, J. A.; Darjuan, M. M.; Mercer, J. E.; Chen, S.; van der Meel, R.; Thewalt, J. L.; Tam, Y. Y. C.; Cullis, P. R. On the Formation and Morphology of Lipid Nanoparticles Containing Ionizable Cationic Lipids and SiRNA. *ACS Nano* **2018**, *12* (5), 4787–4795. https://doi.org/10.1021/acsnano.8b01516.

(29) Huang, X.; Chau, Y. Investigating Impacts of Surface Charge on Intraocular Distribution of Intravitreal Lipid Nanoparticles. *Exp. Eye Res.* **2019**, *186*, 107711. https://doi.org/10.1016/j.exer.2019.107711.

(30) Kim, H.; Robinson, S. B.; Csaky, K. G. Investigating the Movement of Intravitreal Human Serum Albumin Nanoparticles in the Vitreous and Retina. *Pharm. Res.* **2009**, *26* (2), 329–337. https://doi.org/10.1007/s11095-008-9745-6.

(31) Let's Talk about Lipid Nanoparticles. *Nat. Rev. Mater.* **2021**, *6* (2), 99–99. https://doi.org/10.1038/s41578-021-00281-4.

(32) Lv, H.; Zhang, S.; Wang, B.; Cui, S.; Yan, J. Toxicity of Cationic Lipids and Cationic Polymers in Gene Delivery. *J. Controlled Release* **2006**, *114* (1), 100–109. https://doi.org/10.1016/j.jconrel.2006.04.014.

(33) Patel, S.; Ashwanikumar, N.; Robinson, E.; Xia, Y.; Mihai, C.; Griffith, J. P.; Hou, S.; Esposito, A. A.; Ketova, T.; Welsher, K.; Joyal, J. L.; Almarsson, Ö.; Sahay, G. Naturally-Occurring Cholesterol Analogues in Lipid Nanoparticles Induce Polymorphic Shape and Enhance Intracellular Delivery of MRNA. *Nat. Commun.* **2020**, *11* (1), 983. https://doi.org/10.1038/s41467-020-14527-2.

(34) Kranz, L. M.; Diken, M.; Haas, H.; Kreiter, S.; Loquai, C.; Reuter, K. C.; Meng, M.; Fritz, D.; Vascotto, F.; Hefesha, H.; Grunwitz, C.; Vormehr, M.; Hüsemann, Y.; Selmi, A.; Kuhn, A. N.; Buck, J.; Derhovanessian, E.; Rae, R.; Attig, S.; Diekmann, J.; Jabulowsky, R. A.; Heesch, S.; Hassel, J.; Langguth, P.; Grabbe, S.; Huber, C.; Türeci, Ö.; Sahin, U. Systemic RNA Delivery to Dendritic Cells Exploits Antiviral Defence for Cancer Immunotherapy. *Nature* **2016**, *534* (7607), 396–401. https://doi.org/10.1038/nature18300.

(35) Cheng, Q.; Wei, T.; Farbiak, L.; Johnson, L. T.; Dilliard, S. A.; Siegwart, D. J. Selective Organ Targeting (SORT) Nanoparticles for Tissue-Specific MRNA Delivery and CRISPR–Cas Gene Editing. *Nat. Nanotechnol.* **2020**, *15* (4), 313–320. https://doi.org/10.1038/s41565-020-0669-6.
(36) Barba, A. A.; Bochicchio, S.; Dalmoro, A.; Caccavo, D.; Cascone, S.; Lamberti, G. Chapter 10 - Polymeric and Lipid-Based Systems for Controlled Drug Release: An Engineering Point of View. In *Nanomaterials for Drug Delivery and Therapy*; Grumezescu, A. M., Ed.; William Andrew Publishing, 2019; pp 267–304. https://doi.org/10.1016/B978-0-12-816505-8.00013-8.
(37) Makino, K.; Yamada, T.; Kimura, M.; Oka, T.; Ohshima, H.; Kondo, T. Temperature- and Ionic Strength-Induced Conformational Changes in the Lipid Head Group Region of Liposomes as Suggested by Zeta Potential Data. *Biophys. Chem.* **1991**, *41* (2), 175–183. https://doi.org/10.1016/0301-4622(91)80017-L.
(38) Fatouros, D. G.; Klepetsanis, P.; Ioannou, P. V.; Antimisiaris, S. G. The Effect of PH on the Electrophoretic Behaviour of a New Class of Liposomes: Arsonoliposomes. *Int. J. Pharm.* **2005**, *288* (1), 151–156. https://doi.org/10.1016/j.ijpharm.2004.09.016.
(39) Makino, K.; Ohshima, H. Electrophoretic Mobility of a Colloidal Particle with Constant Surface Charge Density. *Langmuir* **2010**, *26* (23), 18016–18019. https://doi.org/10.1021/la1035745.
(40) Oukacine, F.; Morel, A.; Cottet, H. Characterization of Carboxylated Nanolatexes by Capillary Electrophoresis. *Langmuir* **2011**, *27* (7), 4040–4047. https://doi.org/10.1021/la1048562.
(41) Franzen, U.; Østergaard, J. Physico-Chemical Characterization of Liposomes and Drug Substance–Liposome Interactions in Pharmaceutics Using Capillary Electrophoresis and Electrokinetic Chromatography. *J Chromatogr A* **2012**, *1267*, 32–44. https://doi.org/10.1016/j.chroma.2012.07.018.
(42) Franzen, U.; Vermehren, C.; Jensen, H.; Østergaard, J. Physicochemical Characterization of a PEGylated Liposomal Drug Formulation Using Capillary Electrophoresis. *ELECTROPHORESIS* **2011**, *32* (6-7), 738–748. https://doi.org/10.1002/elps.201000552.
(43) Roberts, M. A.; Locascio-Brown, L.; MacCrehan, W. A.; Durst, R. A. Liposome Behavior in Capillary Electrophoresis. *Anal. Chem.* **1996**, *68* (19), 3434–3440. https://doi.org/10.1021/ac9603284.
(44) Wiedmer, S. K.; Jussila, M. S.; Holopainen, J. M.; Alakoskela, J.-M.; Kinnunen, P. K. J.; Riekkola, M.-L. Cholesterol-Containing Phosphatidylcholine Liposomes: Characterization and Use as Dispersed Phase in Electrokinetic Capillary Chromatography. *J. Sep. Sci.* **2002**, *25* (7), 427–437. https://doi.org/10.1002/1615-9314(20020501)25:7<427::AID-JSSC427>3.0.CO;2-#.
(45) Phayre, A. N.; Vanegas Farfano, H. M.; Hayes, M. A. Effects of PH Gradients on Liposomal Charge States Examined by Capillary Electrophoresis. *Langmuir* **2002**, *18* (17), 6499–6503. https://doi.org/10.1021/la025625k.
(46) Chamieh, J.; Davanier, F.; Jannin, V.; Demarne, F.; Cottet, H. Size Characterization of Commercial Micelles and Microemulsions by Taylor Dispersion Analysis. *Int. J. Pharm.* **2015**, *492* (1), 46–54. https://doi.org/10.1016/j.ijpharm.2015.06.037.
(47) Chamieh, J.; Jannin, V.; Demarne, F.; Cottet, H. Hydrodynamic Size Characterization of a Self-Emulsifying Lipid Pharmaceutical Excipient by Taylor Dispersion Analysis with Fluorescent Detection. *Int. J. Pharm.* **2016**, *513* (1), 262–269. https://doi.org/10.1016/j.ijpharm.2016.09.016.
(48) Chamieh, J.; Merdassi, H.; Rossi, J.-C.; Jannin, V.; Demarne, F.; Cottet, H. Size Characterization of Lipid-Based Self-Emulsifying Pharmaceutical Excipients during Lipolysis Using Taylor Dispersion Analysis with Fluorescence Detection. *Int. J. Pharm.* **2018**, *537* (1), 94–101. https://doi.org/10.1016/j.ijpharm.2017.12.032.
(49) Cipelletti, L.; Biron, J.-P.; Martin, M.; Cottet, H. Measuring Arbitrary Diffusion Coefficient Distributions of Nano-Objects by Taylor Dispersion Analysis. *Anal. Chem.* **2015**, *87* (16), 8489–8496. https://doi.org/10.1021/acs.analchem.5b02053.

(50) Zhang, X.; Goel, V.; Robbie, G. J. Pharmacokinetics of Patisiran, the First Approved RNA Interference Therapy in Patients With Hereditary Transthyretin-Mediated Amyloidosis. *J. Clin. Pharmacol.* **2020**, *60* (5), 573–585. https://doi.org/10.1002/jcph.1553.
(51) Urits, I.; Swanson, D.; Swett, M. C.; Patel, A.; Berardino, K.; Amgalan, A.; Berger, A. A.; Kassem, H.; Kaye, A. D.; Viswanath, O. A Review of Patisiran (ONPATTRO®) for the Treatment of Polyneuropathy in People with Hereditary Transthyretin Amyloidosis. *Neurol. Ther.* **2020**, *9* (2), 301–315. https://doi.org/10.1007/s40120-020-00208-1.
(52) Akinc, A.; Maier, M. A.; Manoharan, M.; Fitzgerald, K.; Jayaraman, M.; Barros, S.; Ansell, S.; Du, X.; Hope, M. J.; Madden, T. D.; Mui, B. L.; Semple, S. C.; Tam, Y. K.; Ciufolini, M.; Witzigmann, D.; Kulkarni, J. A.; van der Meel, R.; Cullis, P. R. The Onpattro Story and the Clinical Translation of Nanomedicines Containing Nucleic Acid-Based Drugs. *Nat. Nanotechnol.* **2019**, *14* (12), 1084–1087. https://doi.org/10.1038/s41565-019-0591-y.
(53) Tenchov, R.; Bird, R.; Curtze, A. E.; Zhou, Q. Lipid Nanoparticles—From Liposomes to MRNA Vaccine Delivery, a Landscape of Research Diversity and Advancement. *ACS Nano* **2021**. https://doi.org/10.1021/acsnano.1c04996.
(54) Cheng, X.; Lee, R. J. The Role of Helper Lipids in Lipid Nanoparticles (LNPs) Designed for Oligonucleotide Delivery. *Non-Antigen. Regul. Target. Imaging Ther.* **2016**, *99*, 129–137. https://doi.org/10.1016/j.addr.2016.01.022.
(55) Pozzi, D.; Marchini, C.; Cardarelli, F.; Amenitsch, H.; Garulli, C.; Bifone, A.; Caracciolo, G. Transfection Efficiency Boost of Cholesterol-Containing Lipoplexes. *Biochim. Biophys. Acta BBA - Biomembr.* **2012**, *1818* (9), 2335–2343. https://doi.org/10.1016/j.bbamem.2012.05.017.
(56) Tenchov, B. G.; MacDonald, R. C.; Siegel, D. P. Cubic Phases in Phosphatidylcholine-Cholesterol Mixtures: Cholesterol as Membrane "Fusogen." *Biophys. J.* **2006**, *91* (7), 2508–2516. https://doi.org/10.1529/biophysj.106.083766.
(57) Yanez Arteta, M.; Kjellman, T.; Bartesaghi, S.; Wallin, S.; Wu, X.; Kvist, A. J.; Dabkowska, A.; Székely, N.; Radulescu, A.; Bergenholtz, J.; Lindfors, L. Successful Reprogramming of Cellular Protein Production through MRNA Delivered by Functionalized Lipid Nanoparticles. *Proc. Natl. Acad. Sci.* **2018**, *115* (15), E3351. https://doi.org/10.1073/pnas.1720542115.
(58) Viger-Gravel, J.; Schantz, A.; Pinon, A. C.; Rossini, A. J.; Schantz, S.; Emsley, L. Structure of Lipid Nanoparticles Containing SiRNA or MRNA by Dynamic Nuclear Polarization-Enhanced NMR Spectroscopy. *J. Phys. Chem. B* **2018**, *122* (7), 2073–2081. https://doi.org/10.1021/acs.jpcb.7b10795.
(59) Stetefeld, J.; McKenna, S. A.; Patel, T. R. Dynamic Light Scattering: A Practical Guide and Applications in Biomedical Sciences. *Biophys. Rev.* **2016**, *8* (4), 409–427. https://doi.org/10.1007/s12551-016-0218-6.
(60) Ohshima, H. Approximate Analytic Expression for the Electrophoretic Mobility of a Spherical Colloidal Particle. *J. Colloid Interface Sci.* **2001**, *239* (2), 587–590. https://doi.org/10.1006/jcis.2001.7608.
(61) Ibrahim, A.; Ohshima, H.; Allison, S. A.; Cottet, H. Determination of Effective Charge of Small Ions, Polyelectrolytes and Nanoparticles by Capillary Electrophoresis. *J. Chromatogr. A* **2012**, *1247*, 154–164. https://doi.org/10.1016/j.chroma.2012.05.010.
(62) Ohshima, H.; Furusawa, K.; Dekker, M. Electrical Phenomena at Interfaces : Fundamentals, Measurements and Applications, in Surfactant Science Series - Second Edition. **2018**, *76*, 24–25.

612 **For Table of Contents use only:**

613

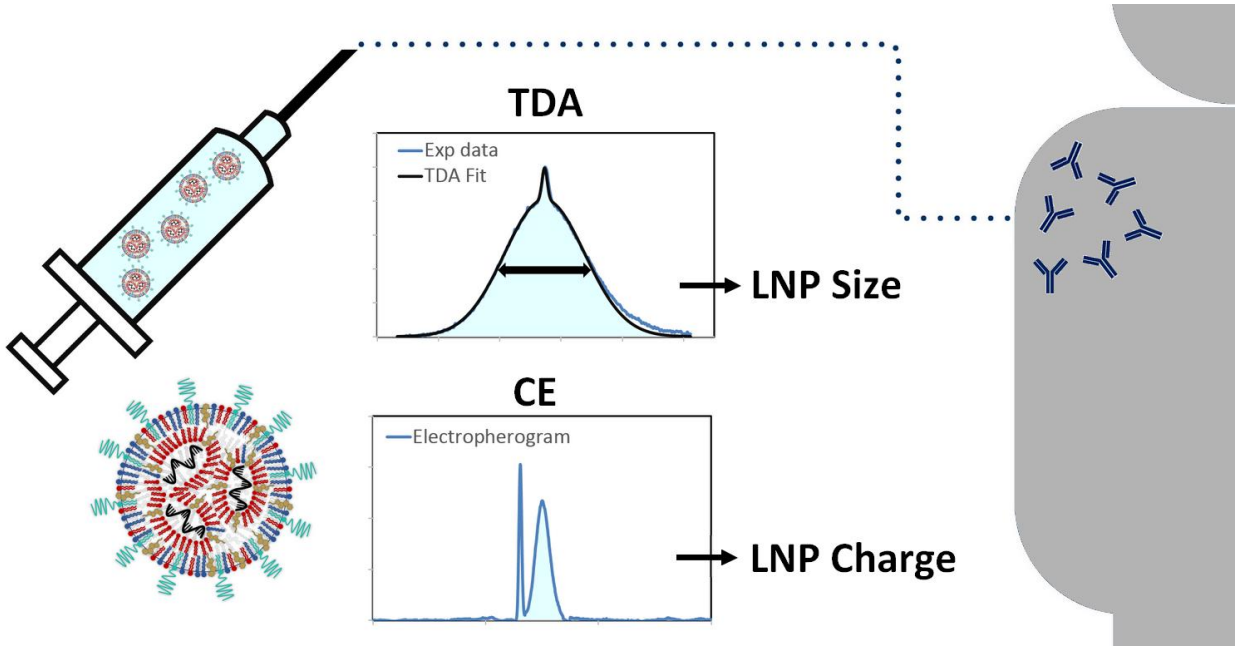

614

615